Proceedings of the 1996 IEEE International
Conference on Control Applications
Dearborn, MI • September 15-18, 1996

Experimental Implementation of Integrator Backstepping and Passive Nonlinear Controllers on the RTAC Testbed

Robert T. Bupp[1], Dennis S. Bernstein[2], and Vincent T. Coppola[3]
Department of Aerospace Engineering, The University of Michigan,
Ann Arbor, Michigan 48109-2118 {rbupp,dsbaero,coppola}@umich.edu

1. Introduction

The Rotational/Translational ACtuator (RTAC) provides a low-dimensional nonlinear system for investigating nonlinear control techniques [1] – [4]. The lossless formulation of this problem involves the nonlinear coupling of an undamped oscillator with a rotational rigid body mode. Stabilization and disturbance rejection objectives for this problem have been formulated as a benchmark problem [3].

We implement four nonlinear controllers on the RTAC, including an integrator backstepping controller and three passivity-based controllers. The integrator backstepping design is based on the work of Wan et al. [1]. This approach requires that the equations of motion be reformulated by partial feedback linearization. Integrator backstepping [5] is then used to produce a family of globally asymptotically stabilizing control laws.

Next, three passivity-based controllers are developed for the RTAC. These controllers have intuitively appealing energy-dissipative properties and thus also inherent stability robustness to plant and disturbance uncertainty. Two of these controllers are encompassed by the classical passivity framework[6], and versions of these controllers have appeared in [2, 3]. The final controller is based upon the novel concept of resetting absorbers [7].

2. Experimental Testbed

A Rotational/Translational ACtuator (RTAC) experimental testbed has been constructed based on the nonlinear system model of [1] – [3] to evaluate the performance of various nonlinear controllers. A photograph of the testbed appears in Figure 1. A model of this arrangement, illustrated by Figure 2, consists of a translational cart of mass M connected by a spring of stiffness k to a wall. The rotational actuator, which is mounted on the cart, consists of a proof mass of mass m and centroidal moment of inertia I mounted at a fixed distance e from its center of rotation. Values of these parameters for the RTAC experiment are given in Table 1. A control torque denoted N is applied to the rotational proof mass, and F denotes a disturbance force.

Let q denote the translational position of the cart from its equilibrium position, and let θ denote the counterclockwise rotational angle of the eccentric mass, where $\theta = 0$ is perpendicular to the direction of translation, as shown in Figure 2. The equations of motion are given by

$$(M+m)\ddot{q} + kq = -me(\ddot{\theta}\cos\theta - \dot{\theta}^2\sin\theta) + F, \quad (1)$$

$$(I+me^2)\ddot{\theta} = -me\ddot{q}\cos\theta + N. \quad (2)$$

Note that while the model is lossless, the experimental testbed experiences unmodeled damping effects such as air friction.

Equations (1) - (2) are given in first-order form by

$$\dot{x} = f(x) + g(x)N, \quad (3)$$

where $x = [q, \dot{q}, \theta, \dot{\theta}]^{\mathrm{T}}$,

$$f(x) = \begin{bmatrix} \dot{q} \\ \frac{-(I+me^2)(kq-me\dot{\theta}^2\sin\theta)}{(M+m)(I+me^2)-(me\cos\theta)^2} \\ \dot{\theta} \\ \frac{me\cos\theta(kq-me\dot{\theta}^2\sin\theta)}{(M+m)(I+me^2)-(me\cos\theta)^2} \end{bmatrix},$$

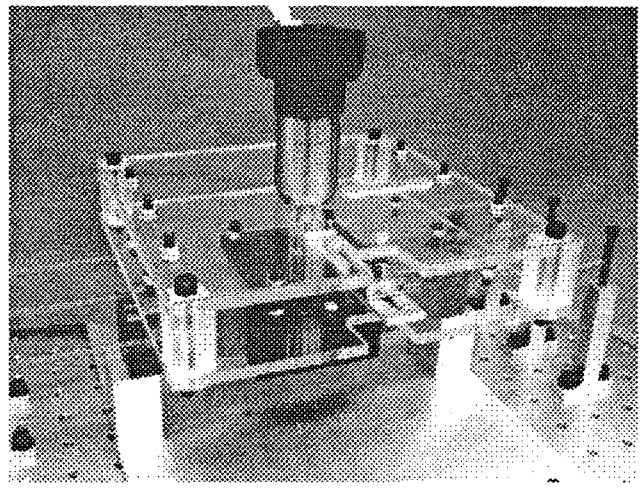

Figure 1: The RTAC Testbed

Cart Mass	M=65 oz
Arm Mass	m=2.44 oz
Spring Constant	k=18.6 oz/in
Eccentricity	e=2.33 in
Arm Inertia	I=0.74 oz-in^2

Table 1: Physical parameters for the RTAC testbed.

[1]Research supported in part by the Air Force Office of Scientific Research under Grant F49620-93-1-0502.
[2]Research supported in part by the Air Force Office of Scientific Research under Grant F49620-95-1-0019.
[3]Research supported in part by NSF Grant MS-9309165.

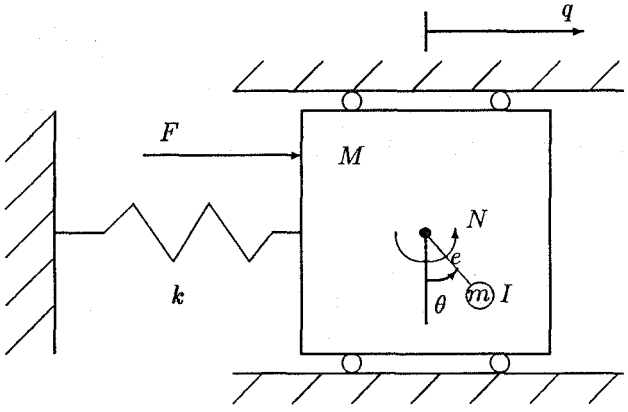

Figure 2: Model of the RTAC Experiment

$$g(x) = \begin{bmatrix} 0 \\ \frac{-me\cos\theta}{(M+m)(I+me^2)-(me\cos\theta)^2} \\ 0 \\ \frac{M+m}{(M+m)(I+me^2)-(me\cos\theta)^2} \end{bmatrix}.$$

A mechanism for generating the disturbance force F for the testbed is currently under design. Hence, $F = 0$ in this paper.

3. Integrator Backstepping Controller

Following the procedure in [8], we normalize the equations of motion, scaling displacement, torque, and time according to

$$\xi \triangleq \sqrt{\frac{M+m}{I+me^2}}q, \nu \triangleq \sqrt{\frac{M+m}{k(I+me^2)}}N, \tau \triangleq \sqrt{\frac{k}{M+m}}t,$$

to obtain

$$\ddot{\xi} + \xi = \varepsilon(\dot{\theta}^2\sin\theta - \ddot{\theta}\cos\theta), \quad (4)$$

$$\ddot{\theta} = -\varepsilon\ddot{\xi}\cos\theta + \nu. \quad (5)$$

In the normalized equations (4) - (5) the parameter ε defined as

$$\varepsilon \triangleq \frac{me}{\sqrt{(I+me^2)(M+m)}} \quad (6)$$

quantifies the coupling between the translational and rotational motions. Note that in this section the notation ( )′ when applied to the scaled variables, denotes differentiation with respect to the scaled time τ.

The control law derived in [8] is given by

$$\begin{aligned}\nu = {} & \left[-(c_1c_2 + \tfrac{p_1}{p_2})(\theta + c_0\arctan(\dot{\xi} + \varepsilon\dot{\theta}\cos\theta)) + \frac{c_0((c_1+c_2)\xi + \dot{\xi})}{1+(\dot{\xi}+\varepsilon\dot{\theta}\cos\theta)^2}\right. \\ & - \frac{\varepsilon p_0(c_2\dot{\xi} + c_2\varepsilon\dot{\theta}\cos\theta - \xi)\left[\sin\theta + \sin(c_0\arctan(\dot{\xi}+\varepsilon\dot{\theta}\cos\theta))\right]}{p_1(\theta + c_0\arctan(\dot{\xi}+\varepsilon\dot{\theta}\cos\theta))} \\ & + \frac{\varepsilon p_0 c_0\xi(\dot{\xi}+\varepsilon\dot{\theta}\cos\theta)\cos(c_0\arctan(\dot{\xi}+\varepsilon\dot{\theta}\cos\theta))}{p_1\left(1+(\dot{\xi}+\varepsilon\dot{\theta}\cos\theta)^2\right)\left(\theta + c_0\arctan(\dot{\xi}+\varepsilon\dot{\theta}\cos\theta)\right)} \\ & + \frac{\varepsilon p_0\dot{\theta}(\dot{\xi}+\varepsilon\dot{\theta}\cos\theta)\left[\sin\theta + \sin(c_0\arctan(\dot{\xi}+\varepsilon\dot{\theta}\cos\theta))\right]}{p_1(\theta + c_0\arctan(\dot{\xi}+\varepsilon\dot{\theta}\cos\theta))^2} \\ & + 2\frac{c_0\xi^2(\dot{\xi}+\varepsilon\dot{\theta}\cos\theta)}{(1+(\dot{\xi}+\varepsilon\dot{\theta}\cos\theta)^2)^2} - \frac{\varepsilon p_0(\dot{\xi}+\varepsilon\dot{\theta}\cos\theta)\dot{\theta}\cos\theta}{p_1(\theta + c_0\arctan(\dot{\xi}+\varepsilon\dot{\theta}\cos\theta))} \\ & \left. -(c_1+c_2)\dot{\theta} - \frac{\varepsilon\cos\theta}{1-\varepsilon^2\cos^2\theta}\left[\xi - \dot{\theta}^2\varepsilon\sin\theta\right]\right](1-\varepsilon^2\cos^2\theta), \end{aligned} \quad (7)$$

where the controller parameters p_0, p_1, p_2, c_0, c_1, and c_2 are all positive, and $0 < c_0 < 2$. Global asymptotic stability of the origin is obtained for every allowable choice of these parameters.

4. Passive Controllers

Our primary objective for controller design is to asymptotically stabilize the origin $x = 0$ of the system (3). In order to exploit the appealing stability robustness property associated with the feedback connection of a passive plant with a passive controller, we must first ensure that the plant to be controlled is passive. In fact, due to the rigid-body rotational mode, the undamped RTAC model (3) is actually *unstable*, and, accordingly, not passive. Therefore, the approach we take for control design is to passify the plant model using bounded state feedback, and then consider various asymptotically stabilizing passive control designs.

To passify the plant model, let $g > 0$ and set

$$N = -mge\sin\theta + u, \quad (8)$$

where the input u will be determined later based on the output of a passive controller. This inner-loop control is chosen because it is a bounded function of the state, and because it will not cause unwinding. The term $-mge\sin\theta$ in (8) lends itself to the interpretation of the gravitational torque that would result if the eccentric arm were in a gravitational field of strength g oriented in the $\theta = 0$ direction. Consequently, the inner-loop system can be viewed as the emulation of a pendulum absorber, which is used, for example, to reduce the vibration levels of tower structures[9]. Tuning of this emulated absorber can be accomplished by adjusting the value of the "gravitational acceleration" parameter g.

With the control (8), (3) becomes

$$\dot{x} = \bar{f}(x) + g(x)u, \quad (9)$$

where

$$\bar{f}(x) = \begin{bmatrix} \dot{q} \\ \frac{-(I+me^2)(kq - me\dot{\theta}^2\sin\theta) + me\cos\theta\, mge\sin\theta}{(M+m)(I+me^2)-(me\cos\theta)^2} \\ \dot{\theta} \\ \frac{me\cos\theta(kq - me\dot{\theta}^2\sin\theta) - (M+m)mge\sin\theta}{(M+m)(I+me^2)-(me\cos\theta)^2} \end{bmatrix}. \quad (10)$$

We take the output to be

$$y = \dot{\theta} \quad (11)$$

so that (9) with input u and output y is passive, with a storage function

$$V_s(x) \triangleq \frac{1}{2}(M+m)\dot{q}^2 - me\dot{q}\dot{\theta}\cos\theta + \frac{1}{2}(I+me^2)\dot{\theta}^2 + \frac{1}{2}kq^2 + mge(1-\cos\theta), \quad (12)$$

and (9), (11) will be termed the *passified plant*.

4.1. Damped Pendulum Absorber Emulation

In this subsection, we design a controller that asymptotically stabilizes the passified plant (9), (11). Let $\alpha, \gamma > 0$, and

$$u = -\alpha\tanh\gamma\dot{\theta}, \quad (13)$$

which has the desirable property of being a bounded function of $\dot{\theta}$. This controller effectively adds a bounded damping term to the pendulum absorber designed in the inner loop, and the resulting controller emulates a damped pendulum absorber. With the control input defined by (8) and (13), the control torque N is bounded in magnitude by $mge + \alpha$.

The closed-loop system (9), (11), (13) is given by

$$\dot{x} = \bar{f}(x) - g(x)\alpha\tanh\gamma\dot{\theta}. \quad (14)$$

By choosing $V(x) = V_s(x)$ to be a Lyapunov candidate, where $V_s(x)$ is given in (12), along the trajectories of the closed-loop system we have

$$\dot{V}(x(t)) = -\alpha\dot{\theta}\tanh\gamma\dot{\theta} \leq 0, \qquad (15)$$

and asymptotic stability of the origin follows from the invariant set theorem [10]. It also follows from the invariant set theorem that the closed-loop trajectory from every initial condition will asymptotically approach an equilibrium position in state space of the form $q = 0$, $\dot{q} = 0$, $\dot{\theta} = 0$, $\theta = n\pi$, $n = 0, \pm 1, \pm 2, \ldots$, which corresponds to one of two physical configurations: a stable configuration corresponding to the arm pointed "down" ($\theta = 0 \bmod 2\pi$), or an unstable configuration corresponding to the arm pointed "up" ($\theta = \pi \bmod 2\pi$). Furthermore, if a particular trajectory tends to asymptotically approach the unstable configuration, a small disturbance would cause it to approach the stable configuration. While this is desirable global behavior, the origin $x = 0$ is not globally asymptotically stable.

4.2. Coupled Pendula Absorber Emulation

In this subsection we extend the emulated damped pendulum absorber design of Section 4.1 to emulate the multi-mode absorber comprised of a system of coupled pendula as shown in Figure 3 [3]. This added flexibility

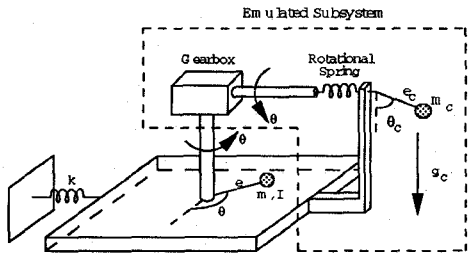

Figure 3: Coupled Pendula Absorber

can be exploited by tuning the controller to effectively reject disturbances with two dominant frequency components, or to efficiently stabilize a multi-mode plant. These capabilities are not explored further in this paper, however.

For the coupled pendulum absorber, the pendulum emulated by the eccentric arm and the damped pendulum control law (13) is termed the *primary pendulum*. The angular motion of the primary pendulum is imagined to be transmitted by a massless rigid rod and ideal gearbox assembly to an *auxiliary pendulum*. A nonlinear rotational spring element is introduced to couple the dynamics of the two pendula. The auxiliary pendulum hangs vertically in an emulated gravitational field of strength g_c, and the damping is represented by $-d_c\dot{\theta}_c$.

The primary pendulum is defined by the parameters m, I, and e, the θ degree of freedom, and controller parameters g, α, and γ as before. The auxiliary pendulum is defined by a virtual mass m_c at a distance e_c about the rotational axis, and the θ_c degree of freedom, measured from the vertical. The inertia of the auxiliary pendulum about the pivot is I_c. The nonlinear rotational spring that couples the primary and auxiliary pendula has restoring torque $-\kappa\sin(\theta_c - \theta)$, where $\kappa > 0$.

To realize the coupled pendula absorber in Figure 3 as a passive compensator, we write the equations of motion with input $y = \dot{\theta}$ and output $-u$ as

$$\dot{x}_c = f_c(x_c) + G_c(x_c)y, \qquad (16)$$
$$-u = h_c(x_c) + J_c(x_c)\phi(x_c, y, t)y, \qquad (17)$$

where $x_c = [\ \theta \quad \theta_c \quad \dot{\theta}_c\ ]^T$, and

$$f_c(x_c) = \begin{bmatrix} 0 \\ \dot{\theta}_c \\ -\frac{\kappa\sin(\theta_c-\theta)}{I_c} - \frac{m_c g_c e_c \sin\theta_c}{I_c} - \frac{d_c}{I_c}\dot{\theta}_c \end{bmatrix},$$

$$G_c(x_c) = [\ 1 \quad 0 \quad 0\ ]^T,$$

$$h_c(x_c) = \kappa\sin(\theta - \theta_c), \quad J_c(x_c) = \alpha,$$

$$\phi(x_c, y, t) = \frac{\tanh\gamma y}{y}.$$

A storage function for the compensator (16)–(17) is given by

$$V_{sc}(x_c) \triangleq \frac{1}{2}I_c\dot{\theta}_c^2 + m_c g_c e_c(1 - \cos\theta_c) + \kappa(1 - \cos(\theta - \theta_c)).$$

Asymptotic stability of the closed-loop system follows from the invariant set theorem, where $V_{cl}(x, x_c) = V_s(x) + V_{sc}(x_c)$ is used as a Lyapunov function for the closed-loop system. It also follows from the invariant set theorem that the stability properties of the equilibria $q = 0$, $\dot{q} = 0$, $\dot{\theta} = 0$, $\dot{\theta}_c = 0$ $\theta = \pm n_1\pi$, $\theta_c = \pm n_2\pi$ for integers n_1 and n_2, are qualitatively similar to those of the closed-loop system involving the damped pendulum absorber of Section 4.1 in that all closed-loop trajectories asymptotically approach the origin, modulo π in the rotational states θ, θ_c.

4.3. Virtual Resetting Absorber Controllers

The third dissipative controller we consider is a virtual resetting absorber controller, which emulates an absorber system whose states are reset to achieve instantaneous reduction of the "total energy" of the closed-loop system, where the total energy includes the kinetic and potential energies associated with the actual physical plant, as well as the *emulated energy* associated with the states of the controller. One type of virtual resetting controller, called a *virtual trap-door absorber* is described in [7], where the resetting algorithm is used to achieve finite-time stabilization of the double integrator. A general theory of virtual resetting absorber controllers is developed in [11]. Resetting differential systems are also considered in [12].

Resetting differential systems consist of three main elements: a continuous-time dynamical equation, which governs the motion of the system between resetting events; a difference equation, which governs the way the states of the controller are instantaneously changed when a resetting event occurs; and a condition that determines when the states of the system are to be reset. The evolution of the state of a resetting differential system is as follows: when the resetting condition is not met, the state corresponds to the solution of the differential equation, with appropriate initial conditions. Upon reaching a point in time and/or state space that satisfies the resetting condition, the state of the system is instantly reset according to the resetting law. The state then proceeds to evolve as a solution of the differential equation again, until the resetting condition is again satisfied.

Our resetting controller is given by

$$\dot{x}_c = \begin{bmatrix} \dot{\theta}_c \\ -\frac{\kappa}{I_c}\sin(\theta_c - \theta) \end{bmatrix}, \quad \kappa \sin(\theta - \theta_c)\dot{\theta} > 0, \quad (18)$$

$$\Delta x_c = \begin{bmatrix} \theta - \theta_c \\ -\dot{\theta}_c \end{bmatrix}, \kappa \sin(\theta - \theta_c)\dot{\theta} \leq 0, \quad (19)$$

$$u = \kappa \sin(\theta_c - \theta). \quad (20)$$

The continuous-time equation governing the behavior of the state x_c between resetting events is given by (18). These dynamics represent the coupled pendula absorber of Section 4.2 where the gravity term g_c and the dissipation term d_c are both set to zero. Notice that unlike the passive controller designs of sections 4.1 and 4.2, this controller has no dissipation term in its dynamics (18).

The resetting law given by (19) describes the instantaneous change in the controller state that occurs when the resetting condition is met; that is, when the resetting condition is met, the state x_c is instantly reset to $x_c + \Delta x_s$, and thus according to (19), θ_c is reset to $\theta_c + \theta - \theta_c = \theta$, and $\dot{\theta}_c$ is reset to $\dot{\theta}_c - \dot{\theta}_c = 0$. This resetting law (19) thus resets θ_c to θ and $\dot{\theta}_c$ to 0.

The resetting condition in (18)–(19) involves a sign condition on the function $\kappa \sin(\theta - \theta_c)\dot{\theta}$. The motivation for this condition, as well as for the form of the reset law (19), is based on properties of the emulated energy.

The emulated energy is given by

$$V_c(x_c, x) = \frac{1}{2} I_c \dot{\theta}_c^2 + \kappa(1 - \cos(\theta - \theta_c)) \geq 0, \quad (21)$$

and in the closed loop,

$$\frac{d}{dt} V_c(x_c, x) = \kappa \sin(\theta - \theta_c)\dot{\theta}. \quad (22)$$

It follows from (9)–(12) and (18)–(22) that

$$\frac{d}{dt} V_s(x) = \dot{\theta} u = \kappa \sin(\theta - \theta_c)\dot{\theta} = -\frac{d}{dt} V_c(x_c, x). \quad (23)$$

Thus, increasing V_c corresponds to decreasing V_s. It is now clear from (18)–(19) and (22) that the resetting condition is chosen so that the states of the controller evolve without resetting as long as the emulated energy is increasing; that is, no resetting occurs provided the controller is removing energy from the RTAC. When the controller is no longer able to remove energy from the RTAC, the controller states are reset. This change in controller state causes the emulated energy (21) to be instantly transferred from $V_c(x_c, x) \geq 0$ to $V_c(x_c + \Delta x_c, x) = 0$, effectively dumping any "energy" that had accumulated in the controller.

In this approach, energy is allowed to flow from the plant into the controller, but due to the resetting mechanism, no energy can flow from the controller back to the plant. To implement the *one-way absorber* controller on the RTAC, only the angle θ is measured. The value of the compensator energy (21) is evaluated at each time step, and the controller states are reset whenever the current value of the compensator energy is less than or equal to its previous value.

5. Experimental Results

In this section, the controller designs of Section 3 and Section 4 are implemented and evaluated on the RTAC testbed. The baseline experiment used to evaluate the performance of the controllers is an initial condition response, where $q(0) = 1.5''$, $\dot{q}(0) = 0$. For the passivity-based controllers, the arm is set initially to $\theta = 0$ and $\dot{\theta}(0) = 0$. The RTAC is held in this initial configuration, with the controller active and no control torque results. The experiment begins when the cart is released. For the integrator backstepping controller, when the cart is held motionless at $q(0) = 1.5''$, control torques cause the arm to be initially at rest at approximately $\theta = 145°$.

For each experiment, a settling time is computed as the time required for the cart displacement to become less than 10% of the initial value, or 0.15″. An approximate damping ratio is assigned to each response based on logarithmic decrement analysis. A summary of the results is tabulated in Table 2. Clearly, the responses of these nonlinear systems are not expected to mimic the responses of a linear system. However, by approximating the rate of decrease of the amplitude of the cart displacement during roughly the first five seconds of the experiment, a damping ratio can be assigned that is useful for comparison purposes.

The integrator backstepping controller described in Section 3 is implemented with $p_0 = 5000$, $p_1 = 500$, $p_2 = 500$, $c_0 = 0.5$, $c_1 = 1$, and $c_2 = 1$. These parameters were selected by trial and error, as it is not clear precisely what role is played by the individual controller parameters in determining the closed-loop response. The experimental initial-condition response is shown in Figure 4, and performance is summarized in Table 2. It is evident that the controller is able to bring the cart and arm to rest at the desired zero position. The controller output is characterized by a large amplitude control signal — saturating often during the initial two seconds — with substantial high frequency content.

The damped pendulum absorber described in Section 4.1 is designed with $m = 3.4$ oz, $g = 19.7$ ft/sec^2, $e = 2.33$ in, $\alpha = 10$ oz-in, and $\gamma = 0.0057$ sec. The parameters m and e are chosen to approximately reflect the actual mass and eccentricity of the arm. The parameter g is tuned so that, in the absence of damping, the initial condition response of the cart excites the greatest amount of motion in the arm. This procedure helps tune the natural frequency of the absorber to the natural frequency of the cart, which is useful for efficiently transferring the energy from the cart to the arm where it can be dissipated. The parameter α is chosen first to set the torque bound, while the damping parameter γ is tuned to provide adequate damping. If γ is too large then the energy transfer from the cart to the arm becomes greatly reduced, whereas if γ is too small then energy is transferred but not dissipated. The response to the baseline initial condition is given in Figure 5, and settling performance is summarized in Table 2. Residual oscillations of approximately 0.04″ amplitude are not damped by the controller.

The coupled pendula absorber described in Section 4.2 is designed with $m = 3.4$ oz, $g = 34.6$ ft/sec^2, $e = 2.33$ in, $\alpha = 10$ oz-in, $\gamma = 0.0057$ sec, $\kappa = 14.2$ oz-in, $I_c = 11.3$ oz-in^2, $e_c = 0$, and $d_c = 14.2$ oz-in-sec. Here again the parameters m and e are chosen to reflect the actual mass and eccentricity of the arm. To achieve good settling behavior, the parameters are tuned so that the initial condition response of the cart excites

one "mode" of the coupled pendulum absorber system as much as possible. The response to the baseline initial condition is given in Figure 6, and performance is summarized in Table 2. Residual oscillations of approximately 0.1" amplitude are not damped by the controller.

The one-way absorber controller described in Section 4.3 is designed with $m = 3.4$ oz, $g = 19.7$ ft/sec^2, $e = 2.33$ in, $\kappa = 4.25$ oz-in, and $I_c = 1.1$ oz-in^2. As was the case for the previous absorber-based controllers, the parameters m and e are chosen to reflect the actual mass and eccentricity of the arm. As it was for the damped pendulum absorber controller, the parameter g is chosen to allow the most efficient energy transfer from the cart to the eccentric arm. Now instead of proceeding to the selection of the proper dashpot parameter as we did in the damped pendulum absorber design, we simply design the controller parameters κ and I_c to exchange energy efficiently with the eccentric arm. The response of the one-way absorber controller to the baseline initial condition is given in Figure 7, and performance is summarized in Table 2. Residual cart oscillation of 0.08" amplitude are not damped by the controller. Some discontinuity in the control signal due to the resetting nature of this controller is apparent in the figure.

It has been noted in all of the passivity-based control cases that there is a residual oscillation of the cart that the controllers cannot remove. This is due to stiction in the motor/arm assembly which is not included in the dynamical model. For oscillations of this level, the accelerations of the cart are so small that the stiction force alone keeps the arm from moving, and without motion in the arm, energy cannot be removed from the cart. To contrast, the integrator backstepping controller, being a full-state-feedback control law, applies torque based on measured cart displacement and velocity, and thus, despite the presence of stiction, can remove the low amplitude cart oscillations that the passive controllers cannot.

It is to be expected that the integrator backstepping controller could achieve better performance than the absorber-based controllers, since the former was not restricted by passivity constraints. In fact, simulations indicate that the integrator backstepping controller can achieve much lower settling times compared to passive designs. However, due to the control amplitude constraint imposed to safeguard the actuator, these high authority integrator backstepping controllers could not be implemented, and, although as implemented they used 25 times more control torque, the integrator backstepping controller was only able to achieve settling behavior roughly comparable to the absorber-based controllers.

While the passive controllers do not reach the maximum torque constraint, they also cannot make use of the extra available torque. The best performance of these absorber-based controllers is achieved by careful tuning of the control parameters, and "increasing the gain" only serves to detune the controller. A controller that more efficiently uses the available torque to improve the settling performance of the RTAC would be desirable.

Controller	ζ_{approx}	u_{max}
Integrator Backstepping	3.7%	12.2 oz-in (saturated)
Damped Pendulum Absorber	5.1%	0.47 oz-in
Coupled Pendula Absorber	3.2%	0.52 oz-in
Virtual Resetting Absorber	5.2%	0.44 oz-in

Table 2: Summary of controller performance

References

[1] C.-J. Wan, D. S. Bernstein, and V. T. Coppola, "Global Stabilization of the Oscillating Eccentric Rotor," *Proc. IEEE Conf. Dec. Contr.*, pp. 4024 - 4029, Orlando, FL, December 1994. Also *Nonlin. Dyn.*, Vol. 10, pp. 49–62, 1996.

[2] R. T. Bupp, C.-J. Wan, V. T. Coppola, and D. S. Bernstein, "Design of a Rotational Actuator for Global Stabilization of Translational Motion," *Proc. ASME Winter Meeting, DE-Vol 75*, pp. 449 - 456, Chicago, IL, November 1994.

[3] R. T. Bupp, D. S. Bernstein, and V. T. Coppola, "A Benchmark Problem for Nonlinear Control Design: Problem Statement, Experimental Testbed, and Passive Nonlinear Compensation," *Proc. Amer. Contr. Conf.*, pp. 4363–4367, Seattle, WA, June 1995.

[4] M. Jankovic, D. Fontaine, and P. V. Kokotović, "TORA Example: Cascade- and Passivity-Based Control Designs," *IEEE Contr. Sys. Tech.*, Vol. 4, No. 3, pp. 292 - 297, 1996.

[5] I. Kanellakopoulos, P. V. Kokotović, and A. S. Morse, "A Toolkit for Nonlinear Feedback Design," *Sys. Contr. Lett.*, Vol. 18, pp. 83–92, 1992.

[6] P. J. Moylan, "Implications of Passivity in a Class of Nonlinear Systems," *IEEE Trans. Autom. Contr.*, Vol. 19, No. 4, pp. 373–381, 1974.

[7] R. T. Bupp, D. S. Bernstein, V.-S. Chellaboina, and W. M. Haddad. Finite-Time Stabilization of the Double Integrator Using a Virtual Trap-Door Absorber. Submitted.

[8] C.-J. Wan, D. S. Bernstein, and V. T. Coppola, "Global Stabilization of the Oscillating Eccentric Rotor," *Nonlin. Dyn.*, Vol. 10, pp. 49 - 62, 1996.

[9] B. G. Korenov and L. M. Reznikov. *Dynamic Vibration Absorbers: Theory and Technical Applications.* Wiley, 1993.

[10] M. Vidyasagar. *Nonlinear Systems Analysis.* Prentice Hall, 1978.

[11] R. T. Bupp, D. S. Bernstein, V.-S. Chellaboina, and W. M. Haddad. Virtual Resetting Absorber Controllers: Theory and Applications. In preparation.

[12] V. Lakshmikantham, D. D. Bainov, and P. S. Simeonov. *Theory of Impulsive Differential Equations*, volume 6 of *Series in Modern Applied Mathematics.* World Scientific, Singapore, 1989.

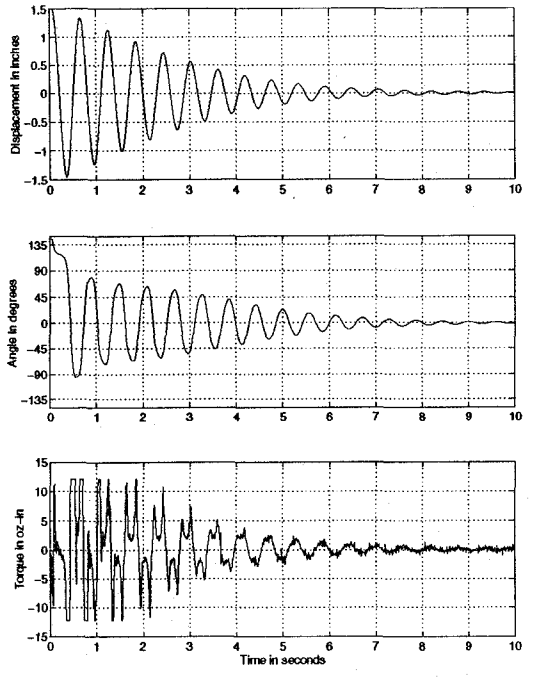

Figure 4: Integrator Backstepping Controller: Response of the RTAC to a 1.5-inch initial displacement.

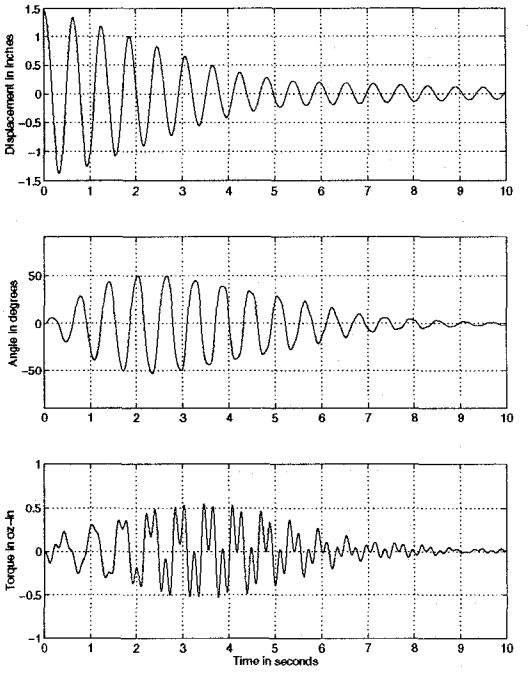

Figure 6: Coupled Pendula Absorber Controller: Response of the RTAC to a 1.5-inch initial displacement.

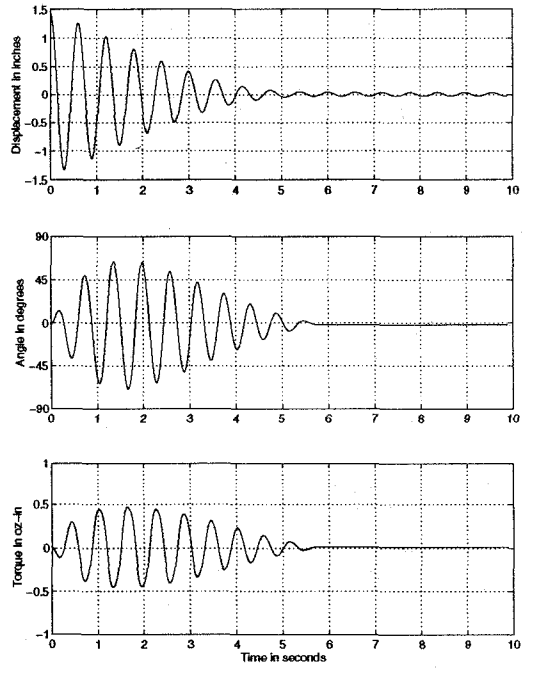

Figure 5: Damped Pendulum Absorber Controller: Response of the RTAC to a 1.5-inch initial displacement.

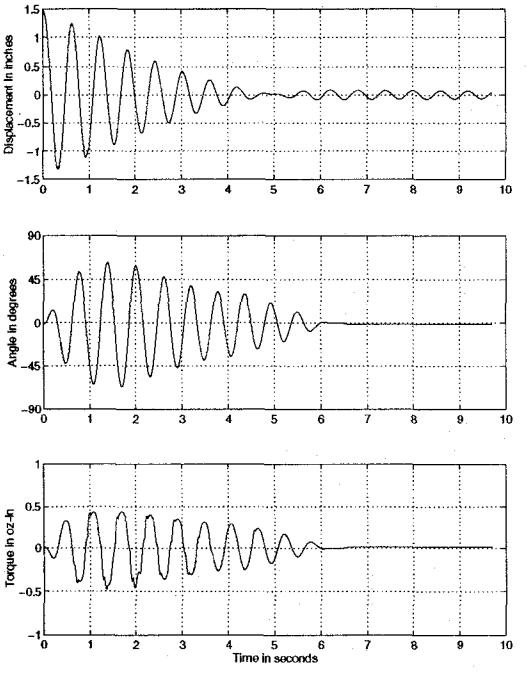

Figure 7: Virtual One-Way Absorber Controller: Response of the RTAC to a 1.5-inch initial displacement.